SCIENTIFIC REPORTS

OPEN

Equatorial Pacific forcing of western Amazonian precipitation during Heinrich Stadial 1

Received: 17 June 2016
Accepted: 07 October 2016
Published: 25 October 2016

Yancheng Zhang[1], Xu Zhang[2], Cristiano M. Chiessi[3], Stefan Mulitza[1], Xiao Zhang[1,†], Gerrit Lohmann[1,2], Matthias Prange[1], Hermann Behling[4], Matthias Zabel[1], Aline Govin[5], André O. Sawakuchi[6], Francisco W. Cruz[6] & Gerold Wefer[1]

Abundant hydroclimatic evidence from western Amazonia and the adjacent Andes documents wet conditions during Heinrich Stadial 1 (HS1, 18–15 ka), a cold period in the high latitudes of the North Atlantic. This precipitation anomaly was attributed to a strengthening of the South American summer monsoon due to a change in the Atlantic interhemispheric sea surface temperature (SST) gradient. However, the physical viability of this mechanism has never been rigorously tested. We address this issue by combining a thorough compilation of tropical South American paleorecords and a set of atmosphere model sensitivity experiments. Our results show that the Atlantic SST variations alone, although leading to dry conditions in northern South America and wet conditions in northeastern Brazil, cannot produce increased precipitation over western Amazonia and the adjacent Andes during HS1. Instead, an eastern equatorial Pacific SST increase (i.e., 0.5–1.5 °C), in response to the slowdown of the Atlantic Meridional Overturning Circulation during HS1, is crucial to generate the wet conditions in these regions. The mechanism works via anomalous low sea level pressure over the eastern equatorial Pacific, which promotes a regional easterly low-level wind anomaly and moisture recycling from central Amazonia towards the Andes.

Amazonia, host of the richest terrestrial biomes on Earth[1–3], plays a fundamental role in the tropical water cycle[4]. Future possible changes of Amazonian precipitation that bear direct consequences on Amazon ecosystems[5,6] and carbon storage[7–9] are of great concern[10]. Analysis of observational data demonstrated a strong dependence of western Amazonian precipitation (e.g., the 2005 drought) on the Atlantic meridional sea surface temperature (SST) gradient[11], but equatorial Pacific climate anomalies have also been related to Amazonian droughts and floods[12,13]. Potential decreases in the strength (by ca. 20–40%[14]) of the Atlantic Meridional Overturning Circulation (AMOC) under climate warming, which involve variations in both the Atlantic meridional SST gradient[15] and the tropical eastern Pacific SST[16], are rationally expected to affect Amazonian precipitation in the future. Past intervals when the AMOC underwent substantial reduction, such as Heinrich Stadial 1 (HS1, 18-15 ka before present, BP), provide valuable information on the response of South American precipitation to a weakened AMOC.

HS1 was characterized as the strongest AMOC perturbation over the last glacial period[17] and significantly influenced tropical South American climate[18–21]. For example, a southward migration of the Intertropical Convergence Zone (ITCZ) during HS1, if compared to the Last Glacial Maximum (LGM, 23-19 ka BP), resulted in a considerable decrease of precipitation over northernmost South America[22,23] and a substantial increase over northeastern (NE) Brazil[24–26]. To explain wet conditions in the Andes[27–29] and southeastern (SE) Brazil[20] during HS1, some authors proposed a strengthening of the South American summer monsoon (SASM) (Fig. 1a). Various freshwater-hosing experiments with climate models of different complexity levels (under both LGM[30]

[1]MARUM – Center for Marine Environmental Sciences, University of Bremen, Germany. [2]Alfred Wegener Institute Helmholtz Centre for Polar and Marine Research, Bremerhaven, Germany. [3]School of Arts, Sciences and Humanities, University of São Paulo, São Paulo, Brazil. [4]Department of Palynology and Climate Dynamics, Albrecht-von-Haller-Institute for Plant Sciences, University of Göttingen, Germany. [5]IPSL/LSCE, Laboratoire des Sciences du Climat et de l'Environnement (CEA-CNRS-UVSQ), Université Paris Saclay, Gif sur Yvette, France. [6]Institute of Geosciences, University of São Paulo, São Paulo, Brazil. †Present address: School of Atmospheric Science, Nanjing University of Information Science and Technology, Nanjing, China. Correspondence and requests for materials should be addressed to Y.Z. (email: yzhang@marum.de)

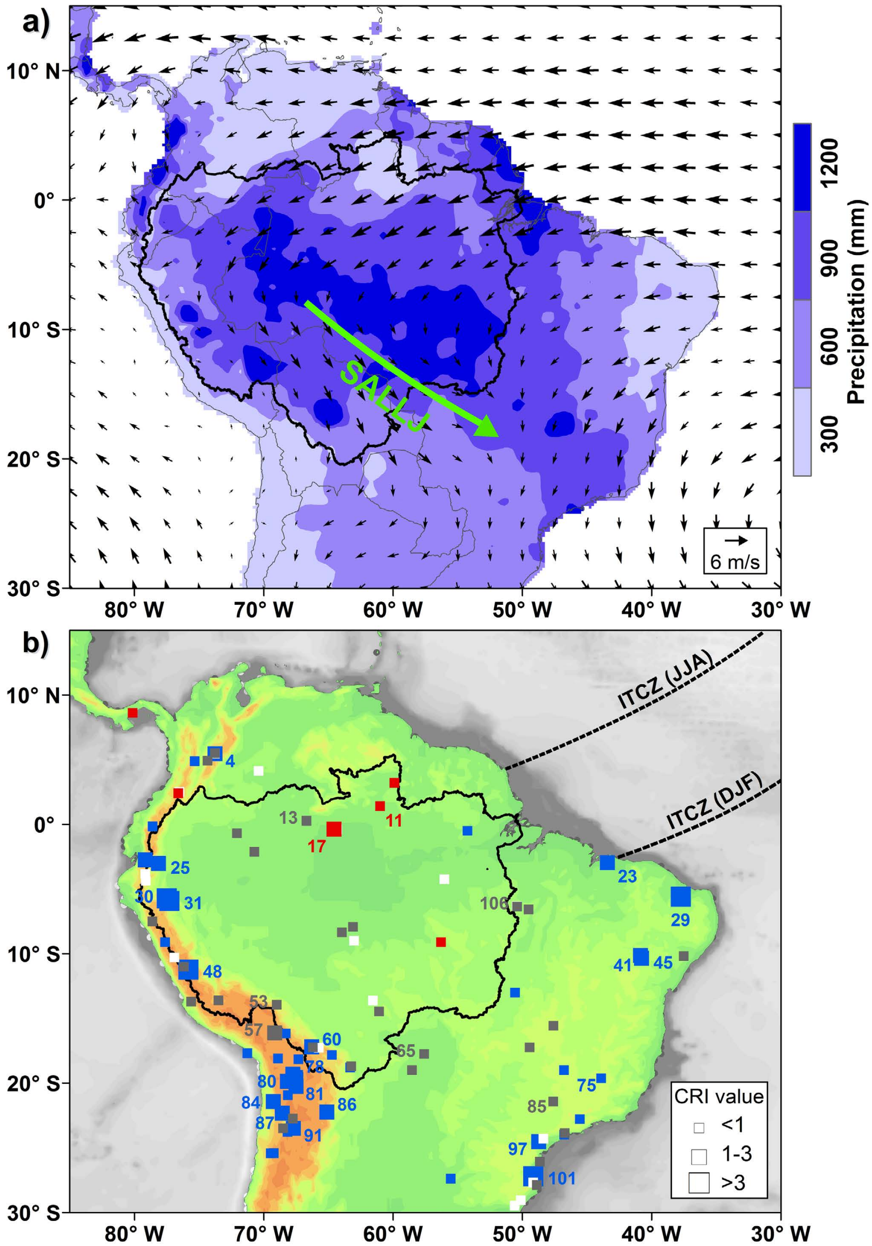

Figure 1. Precipitation and low level atmospheric circulation (**a**) and paleorecords compilation for tropical South America (**b**). (**a**) Long-term (1981–2010) averaged terrestrial precipitation (color scale) from the University of Delaware (http://climate.geog.udel.edu/~climate/) and 850 hPa wind field (vectors) from the NOAA/OAR/ESRL PSD (http://www.esrl.noaa.gov/psd/) during austral summer (December-January-February, DJF). Thick green arrow marks the South American low level jet (SALLJ). (**b**) Compilation of hydroclimate records, expressed as the difference between Heinrich Stadial 1 (HS1, 18-15 ka) and the Last Glacial Maximum (LGM, 23-19 ka). Symbol color indicates drier (red), wetter (blue), similar (grey) and unclear (white) conditions during HS1 in comparison to the LGM. Symbol size denotes the quality of the age model based on the chronological reliability index (CRI) (see Supplementary Information). Paleoclimate records with CRI values > 1 are numbered (Supplementary Table S1). Black dashed lines mark the schematic location of the Intertropical Convergence Zone (ITCZ) during austral summer (DJF) and austral winter (June-July-August, JJA). The Amazon River drainage basin is outlined by the black solid line in both panels (**a**,**b**). The map was plotted by using the ArcGIS software (version 10, https://software.zfn.uni-bremen.de/software/arcgis/).

and modern[31] boundary conditions) successfully simulated the Atlantic ITCZ shift, but exhibited a large spread of rainfall patterns across western Amazonia. In addition, a growing number of studies also suggested a correlation between increased precipitation along the Andes and the El Niño Southern Oscillation (ENSO) during HS1[32–34].

In this study, we integrate (i) a quality-flagged compilation of 107 published hydroclimate records from tropical South America and (ii) a suite of sensitivity experiments in an Atmospheric General Circulation Model

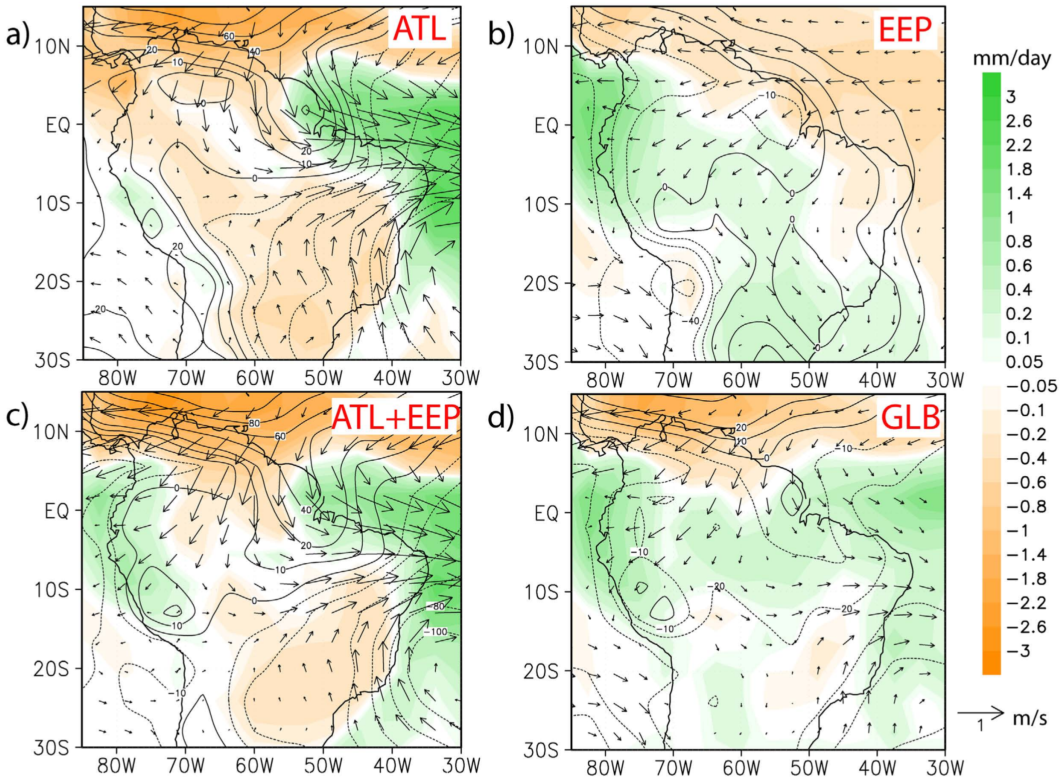

Figure 2. Results of the atmospheric model sensitivity experiments. Differences of simulated (ECHAM5) annual mean climate variables between Heinrich Stadial 1 and the Last Glacial Maximum for the (**a**) Atlantic (ATL) SST experiment, (**b**) eastern equatorial Pacific (EEP) SST experiment, (**c**) combined ATL + EEP experiment and (**d**) global (GLB) SST experiment (see Supplementary Information). Climate variables include rainfall (shaded, mm/day), 850 hPa wind field (vectors, m/s) and sea level pressure (contours, Pa). This map was plotted by using Grid Analysis and Display System (GrADS, Version 2.0.2, http://cola.gmu.edu/grads/grads.php).

(AGCM) to evaluate the impacts of HS1 (relative to the LGM) SST anomalies on tropical South American precipitation (see Materials and Methods). Our results show that SST changes over the eastern equatorial Pacific rather than the Atlantic are responsible for the increased precipitation over western Amazonia and the adjacent Andes during HS1.

Results

Compilation of hydroclimate records. Our compilation of paleomoisture difference between HS1 and the LGM indicates dry conditions to the north of the equator, but widespread wet conditions over the Andes, western Amazonia, NE and SE Brazil (Fig. 1b). Enhanced precipitation (or moisture) extends from the Ecuadorian Andes (e.g., Santiago Cave at ca. 3°S[27]) to the northern Chilean Andes (e.g., central Atacama Desert at 22°S–24°S[35]). The few available records from central Amazonia, characterized by low values of the chronological reliability index (CRI), exhibited in general dry climate during HS1 (Fig. 1b) (see Supplementary Information).

Atmosphere model sensitivity experiments. The sensitivity experiments in this study were performed by using an atmosphere general circulation model (AGCM), the ECHAM5 (see Materials and Methods for a detailed design of model simulations). Driving the AGCM with global HS1 SST anomalies (see Supplementary Fig. S4) in the global SST experiment (Fig. 2d) shows comparable rainfall regimes to the ones simulated by the fully coupled atmosphere-ocean model[36] (Supplementary Fig. S3). The ATL SST experiment that was forced by only Atlantic HS1 SST anomalies simulates a southward migration of the ITCZ, as evidenced by decreased rainfall over northernmost South America and increased rainfall over NE Brazil (Fig. 2a), but apparently fails to generate the wet conditions over western Amazonia. The EEP SST experiment (by applying only eastern equatorial Pacific HS1 SST anomalies) produces enhanced rainfall over western Amazonia together with the intensification of the northeast trade winds over central Amazonia and the South American Low Level Jet (SALLJ) (Fig. 2b), while the ITCZ displays no evident shift. The ATL + EEP SST experiment, in which we superimposed the eastern equatorial Pacific SST anomalies upon the Atlantic interhemispheric SST gradient, exhibits increased rainfall and easterly wind anomalies over western Amazonia (Fig. 2c), although dry conditions over SE Brazil are in contradiction to the GLB SST and the EEP SST experiments (Fig. 2b,d) as well as to our hydroclimate compilation (Fig. 1b).

Discussion

During HS1, a stronger SASM associated with a change in the Atlantic interhemispheric SST gradient was commonly assumed to have triggered increased precipitation over the Amazonian Andes[27–29]. By contrast, our ATL SST experiment shows that the change in Atlantic interhemispheric SST gradient actually weakens the northeast trade winds over central Amazonia and the SALLJ (Fig. 2a), such that less moisture is transported from the tropical Atlantic towards western Amazonia and the adjacent Andes (Fig. 2a). Decreased precipitation over these areas as reproduced by the ATL SST experiment (Fig. 2a), however, conflicts with the prevailing wet conditions derived from our compilation (Fig. 1b). Thus, the Atlantic interhemispheric SST gradient alone is insufficient to explain the wet conditions over western Amazonia and the adjacent Andes during HS1, and contributions from other oceanic regions (e.g., tropical Pacific) should be taken into account.

The EEP SST experiment demonstrates that positive climatological SST anomalies over the eastern equatorial Pacific (Supplementary Fig. S4) are able to cause increased precipitation over western Amazonia and the adjacent Andes during HS1, probably in relation to enhanced northeast trade winds over central Amazonia and the SALLJ (Fig. 2b). Intensified northeast trade winds over central Amazonia, importantly, are also clearly identified in the ATL + EEP SST experiment (Fig. 2c). Remarkably, the wind field pattern over the western tropical Atlantic from the ATL + EEP SST experiment rather resembles that of the ATL SST experiment than of the EEP SST experiment (Fig. 2a,c). This result implies that in the ATL + EEP SST experiment, western Amazonia and the adjacent Andes still experienced an increased rainfall, although less equatorial Atlantic moisture was transported towards the Andes. These features agree well with the overall characteristics of our compilation (Fig. 1b), in particular with the presence of dry conditions over central Amazonia during HS1.

If the Atlantic meridional SST gradient was not the only driver for increased rainfall over the Amazonian Andes[37–39], other processes must be involved. We turn to the SST increases of around 0.5-1.5 °C in the eastern equatorial Pacific during HS1, with the exception of minor SST decreases over coastal regions[40,41] (Supplementary Fig. S4 and Table S2). These SST variations tend to yield low-pressure anomalies over the eastern equatorial Pacific, which then deepens the zonal sea level pressure (SLP) gradient between the Atlantic and the Pacific and strengthens the easterly flow anomaly over western Amazonia and the adjacent Andes (Fig. 2b–d). Such easterly wind anomalies together with the northeast trade winds over central Amazonia subsequently promote moisture recycling from central Amazonia towards the Andes, enhancing the evaporation-condensation along its pathway[42] (as sketched in Supplementary Fig. S5). In fact, this mechanism was previously suggested to account for the wet Andean conditions during the LGM[42], with a particular consideration of the Andes topography (Supplementary Fig. S9). The extent to which enhanced moisture recycling contributed to the wet conditions over the Amazonian Andes remains elusive, but our interpretation coincides with abundant evidence across the central Andes that substantiated increased proportions of regional-sourced moisture over HS1 and the LGM[32–35,43–46].

Seasonal-scale SST changes in the eastern equatorial Pacific (Supplementary Figs S6 and S7) were often assigned to ENSO activity[47]. Because reconstructions of the ENSO variability across HS1 and the LGM were so far not well established from both numerical simulations[48,49] and proxy data[50–52], it is difficult to quantify the ENSO impact on South American precipitation during HS1. For instance, rainfall over NE Brazil and SE Brazil, which are today typically in strong negative and positive relationship with El Niño events[53], indeed experienced similar wet patterns during HS1 (Fig. 1b). Analyses of instrumental data also suggested that climatological conditions over the eastern equatorial Pacific (e.g., related to ENSO[52]) may be linked to Atlantic climate forcing[54,55]. Eastern equatorial Pacific SST variations, probably a response to the weakened AMOC during HS1, are, nevertheless, crucial for triggering wet conditions over western Amazonia and the adjacent Andes (Fig. 1b).

Our ATL and ATL + EEP SST experiments (Fig. 2a,c) are unable to produce increased SE Brazilian rainfall as seen in the paleodata during HS1 (Fig. 1b). Interestingly, the GLB SST experiment (Fig. 2d), although forced by global SST anomalies (Supplementary Fig. S4), still cannot capture the wet conditions over SE Brazil. The SALLJ is weakened in both the GLB SST and the ATL + EEP SST experiments (relative to the EEP SST experiment), and thus seems unlikely to transport equatorial Atlantic moisture via western Amazon towards SE Brazil. In a recent paper, Kageyama *et al.*[30] compared eleven freshwater-hosing experiments (under the LGM conditions) with six different fully coupled climate models, none of which, notably, showed increased rainfall over SE Brazil. Therefore, additional investigations on paleoclimate records and model simulations are necessary to clarify this point.

Conclusion

Comparing a compilation of hydroclimate records and atmosphere model sensitivity experiments provides a deeper understanding of the influence of glacial North Atlantic climate on South American precipitation during HS1. An anomalous Atlantic meridional SST gradient, due to AMOC slowdown, drove a southward ITCZ shift leading to decreased precipitation over northernmost South America and increased precipitation over NE Brazil. The concomitant variations in eastern equatorial Pacific SST produced a negative SLP anomaly over the eastern tropical Pacific, which then deepened the SLP gradient between the Atlantic and the Pacific. As a result, it strengthened the northeasterly winds over the central and western Amazonia, enhancing moisture recycling over western Amazonia and the adjacent Andes.

Our results highlight that future changes in the eastern equatorial Pacific SST, as the AMOC weakens, will be of vital importance to affect western Amazonian precipitation. Depending on the magnitude of the AMOC slowdown under different global warming scenarios[10,14], consideration of both the eastern equatorial Pacific and Atlantic SST variations may allow more accurate insights into the possible changes of Amazonian precipitation in the future.

Materials and Methods

Paleomoisture (precipitation) difference between HS1 and the LGM over tropical South America was determined by compiling 107 published terrestrial hydroclimate records between 30°S–10°N and 80°W-35°W, including 53 lacustrine sediment cores, 10 alluvial deposits, 9 speleothems, 9 moraine landforms, 9 fauna remains, 7 shoreline deposits, 5 paleosol sequences, 3 paleodune profiles as well as 2 ice cores. Chronologies and proxies of all these paleorecords were used directly from their original references. To evaluate the dating quality of the selected hydroclimate records, we applied a chronological reliability index (CRI)[56] based on (i) age model properties and (ii) sampling resolution of each record (detailed description is given in Supplementary Information). Higher CRI values indicate more reliable hydroclimate records (Supplementary Fig. S1). By referring to interpretations of proxies in each record individually, we identified four types of paleomoisture (precipitation) anomalies between HS1 and the LGM as: drier, wetter, similar or unclear (Supplementary Fig. S2, Table S1 and Supplementary Information).

To evaluate different regional contributions of climatological SST changes to South American precipitation anomalies between the LGM and HS1 (Supplementary Figs S3–S5), an atmospheric general circulation model (AGCM), the ECHAM5 (L19/T31, i.e., 19 vertical levels and $3.75° \times 3.75°$ horizontal resolution)[57] was employed. Since freshwater perturbation was the major forcing of the AMOC slowdown during HS1[30,58], we used the LGM boundary conditions (i.e., orbital parameters, topography land-sea mask, ice sheet and greenhouse gas concentrations) to operate the experiments in this study. The LGM and HS1 control runs in the AGCM were forced by climatology monthly mean SST and sea ice cover from experiment LGMW and hosing experiment LGMW-0.2 Sv of the fully coupled general circulation model COSMOS (see ref. 36 for further details), respectively. To investigate the individual contributions of SST changes over different basins to South American precipitation anomalies during HS1, we conducted another three sensitivity experiments in which regional SST fields from the experiment LGMW−0.2 Sv[36] were imposed upon the LGMW SST background, such as the Atlantic basin (30°S–80°N) (ATL), the eastern equatorial Pacific (180°E–~70°W, 25°S–25°N) (EEP, Supplementary Fig. S8) and a combination of ATL and EEP (ATL + EEP). The atmosphere model was integrated for 50 years for each model experiment and the last 30 years were taken to calculate climatological fields.

References

1. Silva, J. M. C., Rylands, A. B. & Fonseca, G. A. B. The fate of the Amazonian areas of endemism. *Conservation Biology* **19,** 689–694 (2015).
2. ter Steege, H. *et al.* Hyperdominance in the Amazonian tree flora. *Science* **342,** doi: 10.1126/science.1243092 (2013).
3. Winemiller, K. O. *et al.* Balancing hydropower and biodiversity in the Amazon, Congo, and Mekong. *Science* **351,** 128–129 (2016).
4. Werth, D. & Avissar, R. The local and global effects of Amazon deforestation. *J. Geophys. Res.* **107,** doi: 10.1029/2001JD000717 (2002).
5. Malhi, Y. *et al.* Climate change, deforestation, and the fate of the Amazon. *Science* **390,** 169–172 (2008).
6. Malhi, Y. *et al.* Exploring the likelihood and mechanism of a climate-change-induced dieback of the Amazon rainforest. *Proc. Natl. Acad. Sci. USA* **106,** 20610–20615 (2009).
7. Gatti, L. V. *et al.* Drought sensitivity of Amazonian carbon balance revealed by atmospheric measurements. *Nature* **506,** 76–80 (2014).
8. Brienen, R. J. W. *et al.* Long-term decline of the Amazon carbon sink. *Nature* **519,** 344–348 (2015).
9. Chazdon, R. L. *et al.* Carbon sequestration potential of second-growth forest regeneration in the Latin American tropics. *Sci. Adv.* **2,** doi: 10.1126/sciadv.1501639 (2016).
10. Collins, M. *et al.* In *Climate Change 2013: The Physical Science Basis. Contribution of Working Group I to the Fifth Assessment Report of the Intergovernmental Panel on Climate Change*, (eds Stocker, T. F. *et al.*). Ch. 12, 1029–1136 (Cambridge University Press, 2013).
11. Cox, P. *et al.* Increasing risk of Amazonian drought due to decreasing aerosol pollution. *Nature* **453,** 212–215 (2008).
12. Marengo, J. A. & Espinoza, J. C. Extreme seasonal droughts and floods in Amazonia: causes, trends and impacts. *Int. J. Climatol.* **36,** 1033–1050 (2016).
13. Lopes, A. V., Chiang, J. C. H., Thompson, S. A. & Dracup, J. A. Trend and uncertainty in spatial-temporal patterns of hydrological droughts in the Amazon basin. *Geophys. Res. Lett.* **43,** 3307–3316 (2016).
14. Weaver, A. J. *et al.* Stability of the Atlantic meridional overturning circulation: A model intercomparison. *Geophys. Res. Lett.* **39,** doi: 10.1029/2012GL053763 (2012).
15. Zhang, L. & Wang, C. Multidecadal North Atlantic sea surface temperature and Atlantic meridional overturning circulation variability in CMIP5 historical simulations. *J. Geophys. Res.* **118,** 5772–5791 (2013).
16. Timmermann, A. *et al.* The influence of a weakening of the Atlantic meridional overturning circulation on ENSO. *J. Climate* **20,** 4899–4019 (2007).
17. Böhm, E. *et al.* Strong and deep Atlantic meridional overturning circulation during the last glacial cycle. *Nature* **517,** 73–76 (2015).
18. Hessler, I. *et al.* Millennial-scale changes in vegetation records from tropical Africa and South America during the last glacial. *Quaternary Sci. Rev.* **29,** 2882–2899 (2010).
19. Handiani, D. *et al.* Tropical vegetation response to Heinrich Event 1 as simulated with the UVic ESCM and CCSM3. *Clim. Past* **9,** 1683–1696 (2013).
20. Stríkis, N. M. *et al.* Timing and structure of Mega-SACZ events during Heinrich Stadial 1. *Geophys. Res. Lett.* **42,** 5477–5484 (2015).
21. Mohtadi, M., Prange, M. & Steinke, S. Palaeoclimatic insights into forcing and response of monsoon rainfall. *Nature* **533,** 191–199 (2016).
22. Peterson, L. C., Haug, G. H., Hughen, K. A. & Röhl, U. Rapid changes in the hydrologic cycle of the tropical Atlantic during the Last Glacial. *Science* **290,** 1947–1951 (2000).
23. Deplazes, G. *et al.* Links between tropical rainfall and North Atlantic climate during the last glacial period. *Nat. Geosci.* **6,** 213–217 (2013).
24. Wang, X. *et al.* Northeastern Brazil wet periods linked to distant climate anomalies and rainforest boundary changes. *Nature* **432,** 740–743 (2004).
25. Jaeschke, A., Rühlemann, C., Arz, H. W., Heil, G. & Lohmann, G. Coupling of millennial-scale changes in sea surface temperature and precipitation off northeastern Brazil with high-latitude climate shifts during the last glacial period. *Paleoceanography* **22,** doi: 10.1029/2006PA001391 (2007).
26. Zhang, Y. *et al.* Origin of increased terrigenous supply to the NE-South American continental margin during Heinrich Stadial 1 and the Younger Dryas. *Earth Planet. Sci. Lett.* **432,** 493–500 (2015).
27. Mosblech, N. A. S. *et al.* North Atlantic forcing of Amazonian precipitation during the last ice age. *Nat. Geosci.* **5,** 817–820 (2012).

28. Kanner, L. C., Burns, S. J., Cheng, H. & Edwards, R. L. High latitude forcing of the South American Summer Monsoon during the Last Glacial. *Science* **335,** 570–573 (2012).
29. Cheng, H. *et al.* Climate change patterns in Amazonia and biodiversity. *Nat. Commun.* **4,** doi: 10.1038/ncomms2415 (2013).
30. Kageyama, M. *et al.* Climatic impacts of fresh water hosing under Last Glacial Maximum conditions a multi-model study. *Clim. Past* **9,** 935–953 (2013).
31. Stouffer, R. J. *et al.* Investigating the causes of the response of the thermohaline circulation to past and future climate changes. *J. Climate* **19,** 1365–1387 (2006).
32. Placzek, C., Quade, J. & Patchett, P. J. Geochronology and stratigraphy of late Pleistocene lake cycles on the southern Bolivian Altiplano Implications for causes of tropical climate change. *GSA Bulletin* **118,** 515–532 (2006).
33. Gayo, E. M. *et al.* Late Quaternary hydrological and ecological changes in the hyperarid core of the northern Atacama Desert (~21°S). *Earth-Science Reviews* **113,** 120–140 (2012).
34. Bekaddour, T. *et al.* Paleo erosion rates and climate shifts recorded by Quaternary cut-and-fill sequences in the Pisco valley, central Peru. *Earth Planet. Sci. Lett.* **390,** 103–115 (2014).
35. Betancourt, J. L., Latorre, C., Rech, J. A., Quade, J. & Rylander, K. A. A 22,000-year record of monsoonal precipitation from northern Chile's Atacama desert. *Science* **289,** 1542–1546 (2000).
36. Zhang, X., Lohmann, G., Knorr, G. & Xu, X. Different ocean states and transient characteristics in the Last Glacial Maximum simulations and implications for deglaciation. *Clim. Past* **9,** 2319–2333 (2013).
37. Vuille, M. & Werner, E. M. Stable isotopes in precipitation recording South American summer monsoon and ENSO variability: observations and model results. *Clim. Dyn.* **25,** 401–413 (2005).
38. Lee, J. E., Johnson, K. & Fung, I. Precipitation over South America during the Last Glacial Maximum An analysis of the "amount effect" with a water isotope-enabled general circulation model. *Geophys. Res. Lett.* **36,** doi: 10.1029/2009GL039265 (2009).
39. Baker, P. A. & Fritz, S. C. Nature and causes of Quaternary climate variation of tropical South America. *Quat. Sci. Rev.* **124,** 31–47 (2015).
40. Shakun, J. D. *et al.* Global warming preceded by increasing carbon dioxide concentrations during the last deglaciation. *Nature* **484,** 49–54 (2012).
41. Koutavas, A. & Sachs J. P. Northern timing of deglaciation in the eastern equatorial Pacific from alkenone paleothermometry. *Paleoceanography* **23,** doi: 10.1029/2008PA001593 (2008).
42. Vizy, E. K. & Cook, K. H. Relationship between Amazon and high Andes rainfall. *J. Geophys. Res.* **112,** doi: 10.1029/2006JD007980 (2007).
43. Ammann, C., Jenny, B., Kammer, K. & Messerli, B. Late Quaternary Glacier response to humidity changes in the arid Andes. *Palaeogeogr. Palaeoclimatol. Palaeoecol.* **172,** 313–326 (2001).
44. Godfrey, L. V., Jordan, T. E., Lowenstein, T. K. & Alonso, R. N. Stable isotope constraints on the transport of water to the Andes between 22° and 26°S during the last glacial cycle. *Palaeogeogr. Palaeoclimatol. Palaeoecol.* **194,** 299–317 (2003).
45. Kull, C., Imhof, S., Grosjean, M., Zech, R. & Veit, H. Late Pleistocene glaciation in the Central Andes Temperature versus humidity control - A case study from the eastern Bolivian Andes (17°S) and regional synthesis. *Global Planet. Change* **60,** 148–164 (2008).
46. Thompson, L. G. *et al.* A 25,000-year tropical climate history from Bolivian ice cores. *Science* **282,** 1858–1864 (1998).
47. Stott, L., Poulsen, C., Lund, S. & Thunell, R. Super ENSO and Global Climate Oscillations at Millennial Time Scales. *Science* **297,** 222–226 (2002).
48. Merkel, U., Prange, M. & Schulz, M. ENSO variability and teleconnections during glacial climates. *Quat. Sci. Rev.* **29,** 86–100 (2010).
49. Liu, Z. *et al.* Evolution and forcing mechanisms of El Niño over the past 21,000 years. *Nature* **515,** 550–553 (2014).
50. Koutavas, A., Lynch-Stieglitz, J., Marchitto Jr., T. M. & Sachs, J. P. El Niño-like pattern in Ice Age Tropical Pacific sea surface temperature. *Science* **297,** 226–230 (2002).
51. Felis, T. *et al.* Pronounced interannual variability in tropical South Pacific temperatures during Heinrich Stadial 1. *Nat. Commun.* **3,** doi: 10.1038/ncomms1973 (2012).
52. Ford, H. L., Ravelo, A. C. & Polissar, P. J. Reduced El Niño-Southern Oscillation during the Last Glacial Maximum. *Science* **347,** 255–258 (2015).
53. Grimm, A. M. & Tedeschi, R. G. ENSO and extreme rainfall events in South America. *J. Climate* **22,** 1589–1609 (2009).
54. Dima, M., Lohmann, G. & Rimbu, N. Possible North Atlantic origin for changes in ENSO properties during the 1970s. *Clim. Dyn.* **44,** 925–935 (2015).
55. Wu, L., He, F., Liu, Z. & Li, C. Atmospheric teleconnections of tropical Atlantic variability: interhemispheric, tropical-extratropical, and cross-basin interactions. *J. Climate* **20,** 856–870 (2007).
56. Prado, L. F., Wainer, I., Chiessi, C. M., Ledru, M. P. & Turcq, B. A mid-Holocene climate reconstruction for eastern South America. *Clim. Past* **9,** 2117–2133 (2013).
57. Roeckner, E. *et al. The atmospheric general circulation model ECHAM 5, Part I: Model description. Report 349. Max-Planck Institut für Meteorologie:* Hamburg, Germany (2003).
58. Liu, Z. *et al.* Transient simulation of Last Deglaciation with a new mechanism for Bølling-Allerød warming. *Science* **325,** 310–314 (2009).

Acknowledgements

This work was funded by the Deutsche Forschungsgemeinschaft through the DFG Research Centre/Cluster of Excellence 'The Ocean in the Earth System' and the Helmholtz Climate Initiative REKLIM. We thank two anonymous reviewers for very constructive comments and Dr. Dunia H. Urrego for constructive discussion. X.Z.(Xu) and G.L. were supported by Helmholtz funding through the Polar Regions and Coasts in the Changing Earth System (PACES) programme of Alfred Wegener Institute, and X.Z.(Xu) as well as Helmholtz Postdoc Programme (PD-301) and the national Natural Science Foundation of China (grants 41575067 and 41406220). C.M.C. was supported by FAPESP (grant 2012/17517-3) and CAPES (grants 1976/2014 and 564/2015). A.O.S. acknowledges financial supported from FAPESP (grant 2011/06609-1). The compilation of paleodata presented in this paper will be archived in PANGAEA (www.pangaea.de).

Author Contributions

Y.Z., Xu Z., C.M.C. and S.M. designed the study and wrote the draft. Y.Z. and C.M.C. conducted compilation of the paleodata, Xu Z. and G.L. operated the AGCM for model sensitivity experiments, Xi.Z. and M.P. analyzed additional freshwater hosing experiment, H.B. provided paleorecords for the compilation, M.Z., A.G., A.O.S., F.W.C. and G.W. discussed the results. All authors contributed to interpreting the data and improving the manuscript.

Additional Information

Supplementary information accompanies this paper at http://www.nature.com/srep

Competing financial interests: The authors declare no competing financial interests.

How to cite this article: Zhang, Y. *et al.* Equatorial Pacific forcing of western Amazonian precipitation during Heinrich Stadial 1. *Sci. Rep.* **6**, 35866; doi: 10.1038/srep35866 (2016).

Supplementary information

Equatorial Pacific forcing of western Amazonian precipitation during Heinrich Stadial 1

Yancheng Zhang*, Xu Zhang, Cristiano M. Chiessi, Stefan Mulitza, Xiao Zhang, Gerrit Lohmann, Matthias Prange, Hermann Behling, Matthias Zabel, Aline Govin, André O. Sawakuchi, Francisco W. Cruz, Gerold Wefer

* Correspondence to: yzhang@marum.de

1. Compilation of the hydroclimate records

For the compilation of published paleoclimatic records across tropical South America, we included the following archives: 53 lacustrine sediment cores (geochemistry, palynology and mineralogy), 10 alluvial deposits (geomorphology, palynology), 9 moraine deposits (glacial landforms), 9 speleothems (oxygen stable isotopes), 9 fauna remains (fossil rodent middens, palynology), 7 shoreline deposits (mollusc shells), 5 paleosol sequences (palynology, geochemistry), 3 paleodune profiles (geomorphology, luminescence ages), as well as 2 ice cores (oxygen stable isotopes) (Supplementary Fig.S1). Chronologies (e.g., using ^{14}C, U-Th, luminescence dating methods, as provided in Supplementary Table S1) and interpretation of the hydroclimate records agree to the original reference (Supplementary Table S1).

Fig.S1. Categorization of 107 hydroclimate records based on their chronological reliability index (CRI) values (data and detailed information are given in Supplementary Table S1). The map was plotted using the Microsoft Excel 2010 (https://www.marum.de/en/Microsoft.html).

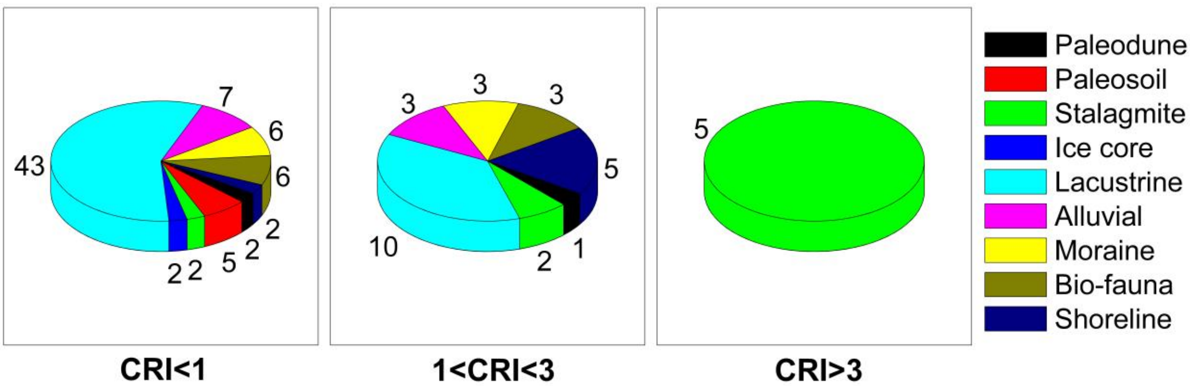

We used the time windows of 18-15 ka (ref. *S1*) and 23-19 ka (ref. *S2*) to define the Heinrich Stadial 1 (HS1) and the Last Glacial Maximum (LGM), respectively. For paleorecords with uncalibrated ^{14}C ages, the intervals of 15-12 ka ^{14}C ages and 20-16 ka ^{14}C ages were used to outline the HS1 and the LGM. Based on the chronological reliability index (CRI) (see below), we mainly used the paleorecords with CRI values over 1 to determine the overall pattern of the paleomoisture difference between HS1 and LGM. We acknowledge that the age controls based on uncalibrated ^{14}C ages may have large uncertainty, because the radiocarbon reservoir correction of terrestrial archives like sediment cores from lacustrine environment are less accurate due to local water-air CO_2 exchange (e.g., ref. *S3*). In the compilation, we included 28 paleoclimate records constrained by uncalibrated ^{14}C ages (with large age uncertainty as mentioned above), but note that only two of them are characterized by CRI values higher than 1 (e.g., sites No.85 and No.91 in Supplementary Table S1). Thus, the consideration of these paleorecords with uncalibrated ^{14}C ages does not modify our conclusions based on the compilation of South American hydroclimate records (Supplementary Fig.S2).

To calculate the CRI values, we employed the function established by Prado et al. (ref. *S4*) as:

$$\mathrm{CRI} = \frac{\mathrm{CA} + \mathrm{D} + \mathrm{R}}{3}$$

where CA (calibration) equals 1 (or 0) if age control points were (or not) calibrated; D (dating) is the number of age control points within HS1 and LGM, divided by 10; R (resolution) refers to the mean number of total samples per entire core length ratio, as given:

$$\mathrm{R} = \begin{cases} 0.1 \text{ for ratio between } 0.01 \text{ and } 0.1 \\ 0.2 \text{ for ratio between } 0.11 \text{ and } 0.2 \\ \qquad\qquad \cdots\cdots \\ 11.0 \text{ for ratio between } 10.01 \text{and } 11.00 \end{cases}$$

Among the selected paleoclimate records, most speleothem records have high CRI values (≥3), while paleoclimatic archives from lacustrine environments (e.g., peat bog, peatland, swamp) or alluvial and moraine deposits generally show low CRI values (Supplementary Table S1, Fig.S1). Based on the interpretation of each paleorecord (see Supplementary Table S1 for further details), we identify the paleomoisture (precipitation) anomalies between HS1 and

LGM with three categories: ‘drier’, ‘wetter’ and ‘similar’. For the paleorecords whose references did not allow a clear comparison (e.g., no information available on paleohydrology variations, or/and no age points available within HS1 or the LGM), we distinguish them as ‘unclear’ (Supplementary Fig.S2, detailed description is given in Supplementary Table S1).

Fig.S2. Types of South American hydroclimatic archives used to determine the difference between Heinrich Stadial 1 (HS1) and the Last Glacial Maximum (LGM) (data are provided in Supplementary Table S1). Red (blue) symbols denote a drier (wetter) HS1 than the LGM, while grey (white) symbols represent similar (unclear) conditions. Symbol sizes relate to the quality level established by chronological reliability index (CRI) (Supplementary Fig.S1). Numbers mark those records with CRI values > 1 (Supplementary Table S1) that constitute the base for the determination of paleomoisture difference between HS1 and the LGM. The map was plotted by using the ArcGIS software (version 10, https://software.zfn.uni-bremen.de/software/arcgis/).

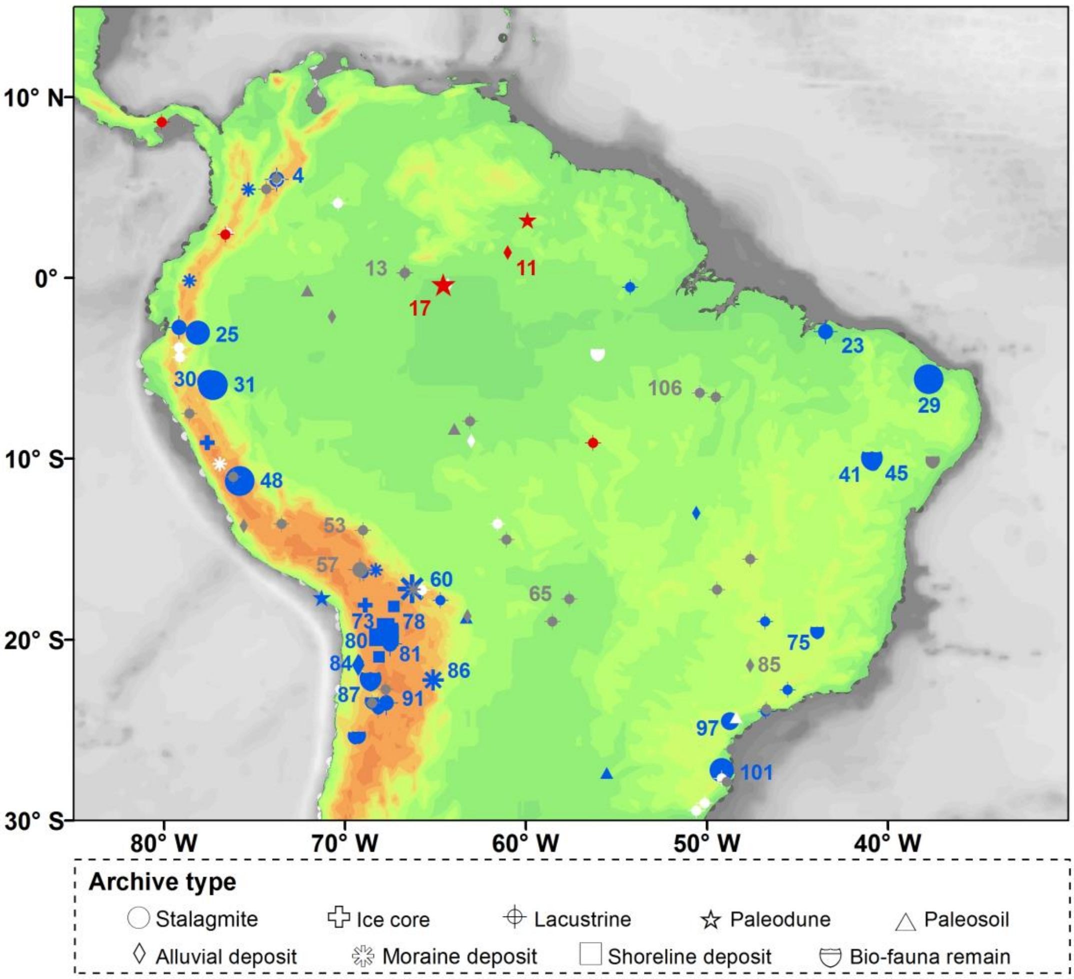

2. General dry HS1 vs. LGM conditions over central Amazonia

Based on palynological analyses, previous studies showed that the dry climate at Lagoa Verde (Hill of six lakes, site No.13; *S5-S6*) and Lagoa da Cachoeira (site No.106; *S7-S8*) was comparable between the LGM and HS1. The paleodune profile at Temedauí, Rio Negro (site No.17; *S9*) apparently demonstrated a slightly enhanced eolian activity during 17.2-16.4 ka compared to the period 22.8-22 ka, both periods being in intensified state relative to the Holocene. Similarly, the megafan at Viruá National Park (site No. 11, *S10*) suggested a high water discharge in wet seasons during 24-20 ka, while an extensive dry season was associated with C4 grassland development between 20-5 ka (with a hiatus during HS1). Together with other paleorecords with low CRI values over central Amazonia (Supplementary Fig.S2, see also Supplementary Table S1 for detailed interpretations), we therefore suggest that central Amazonia underwent slightly drier conditions during HS1 relative to the LGM. A better understanding of this issue depends on new paleoclimate records with high CRI values (e.g., speleothem) from central Amazonia and nearby regions in the future.

Fig.S3. Climatological anomalies between the Heinrich Stadial 1 (HS1) and the Last Glacial Maximum (LGM), as derived from the experiments LGMW-0.2Sv and LGMW in the fully coupled AOGCM respectively (*S11*), including rainfall (shaded, mm/day), 850hPa wind field (vectors, m/s) and sea level pressure (contours, Pa). Good agreement between outputs of the fully coupled AOGCM and the AGCM (Fig.2d in the manuscript), e.g., dry conditions over northernmost South America and wet conditions over the Andes and NE Brazil, suggests that climatological SST variations are a major forcing of South American precipitation changes during HS1. In contrast to both the fully coupled AOGCM (Fig.S3) and the GLB experiment (Fig.2d), our ATL SST experiment shows less precipitation over SE South America (Fig.2c). We suggest that the ATL experiment might underestimate the South Atlantic Convergence Zone rainfall, because it did not include SST changes to the south of 30°S in the Atlantic (see Materials and Methods, supplementary Fig.S4). This map was plotted by using Grid Analysis and Display System (GrADS, Version 2.0.2, http://cola.gmu.edu/grads/grads.php).

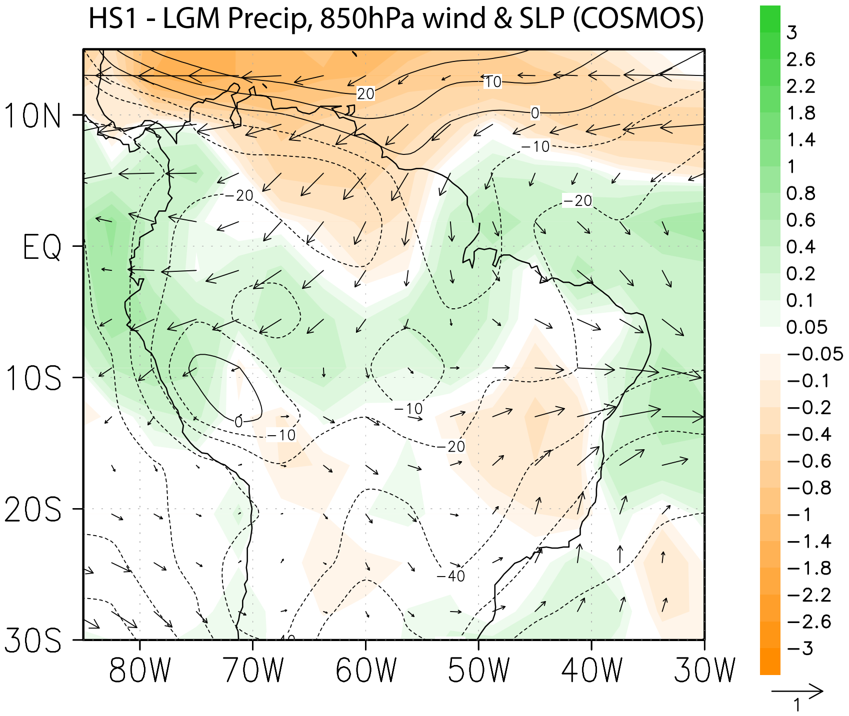

Fig.S4. The COSMOS simulated sea surface temperature (SST) anomalies in the freshwater-hosing experiment (°C) relative to the LGM background experiment (*S11*). The areas outlined within the pink (Atlantic) and black (Pacific) lines were used to perform the ATL SST and EEP SST sensitivity experiments, respectively. Filled circles in the eastern equatorial Pacific denote paleodata-reconstructed SST increases (red) and decreases (blue) during HS1 relative to LGM (data are given in Supplementary Table S2). The map was plotted using the Ocean Data View software (version 4.6.2) (Schlitzer, R., Ocean Data View, http://odv.awi.de, 2015).

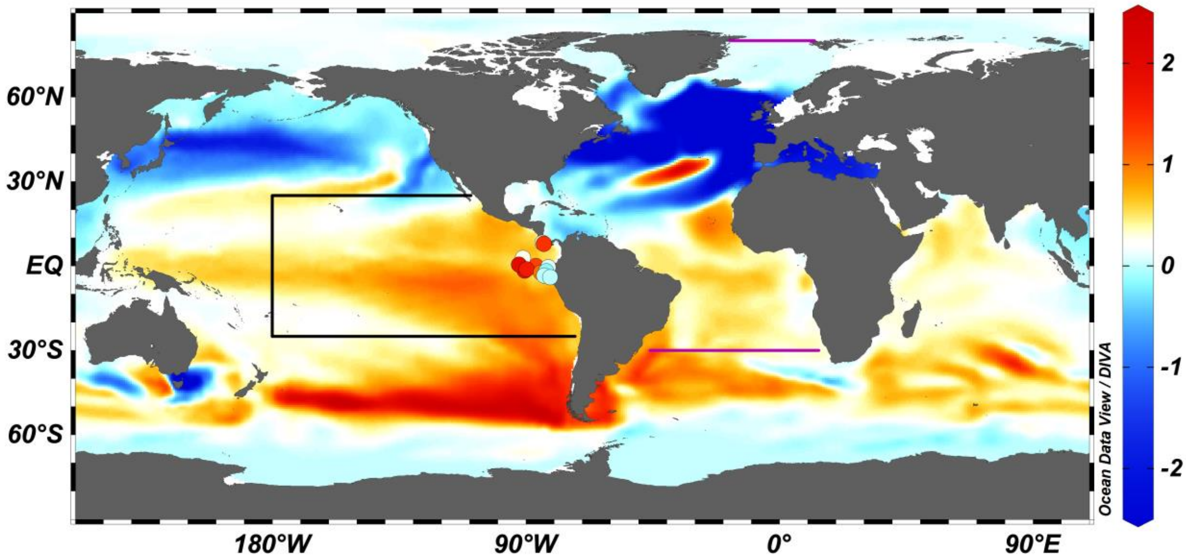

Fig.S5. Schematic map of moisture transport towards the Andes in (a) the ATL experiment and (b) the ATL+EEP experiment. For the ATL experiment, we suppose that less tropical Atlantic moisture is unable to reach the Amazonian Andes directly. In contrast, when the Pacific SST anomalies were forced together with Atlantic SST changes, the tropical Atlantic moisture is further transported from central Amazonia towards the Andes, because of change in sea level pressure gradient between Atlantic and Pacific in the ATL+EEP experiment that leads to an easterly flow from central Amazonia towards the Andes (Fig.2) and then promotes the recycling process of tropical Atlantic moisture. But moisture from both tropical Atlantic and Pacific can hardly cross the Andes due to the steep terrain. The map was plotted by using the ArcGIS software (version 10, https://software.zfn.uni-bremen.de/software/arcgis/).

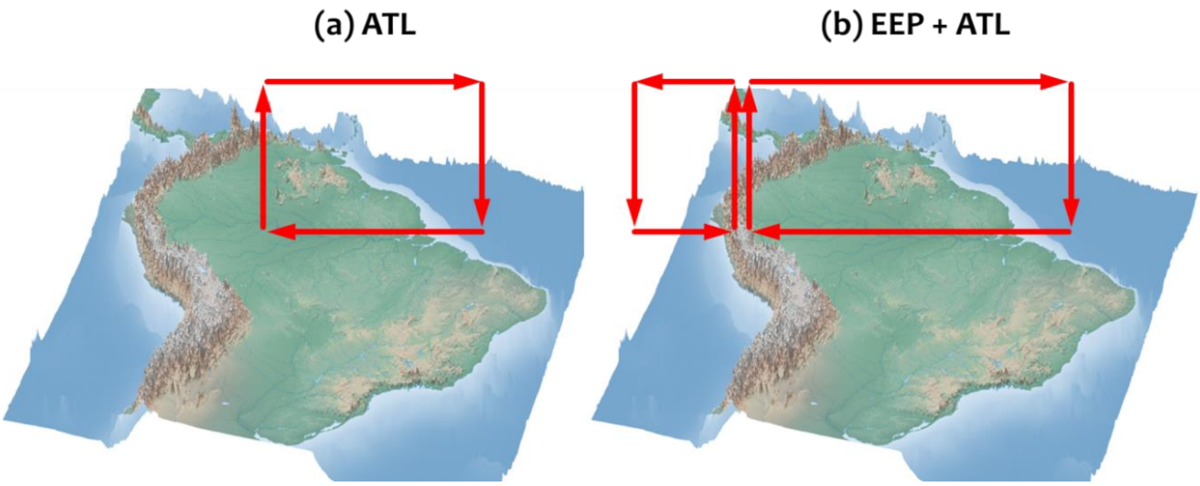

Fig.S6. Wavelet analysis of the El Niño 3.4 SST indices (bounded by 120°W-170°W and 5°S-5°N) from the fully coupled atmosphere-ocean general circulation model (COSMOS, ref. *S11*) for the Last Glacial Maximum (LGM) condition (left) and the freshwater-hosing experiment (right), respectively. The results suggest that the ENSO signal from hosing experiment (thus HS1) is generally characterized by higher frequency (~1 year) and larger variance if compared to the LGM conditions, consistent with other modeling results (ref. *S12-S13*). The wavelet analysis was performed by the Interactive Wavelet Plot (http://ion.exelisvis.com/) and the map was plotted by using the MATLAB software (version R2013b, https://www.marum.de/en/Matlab.html).

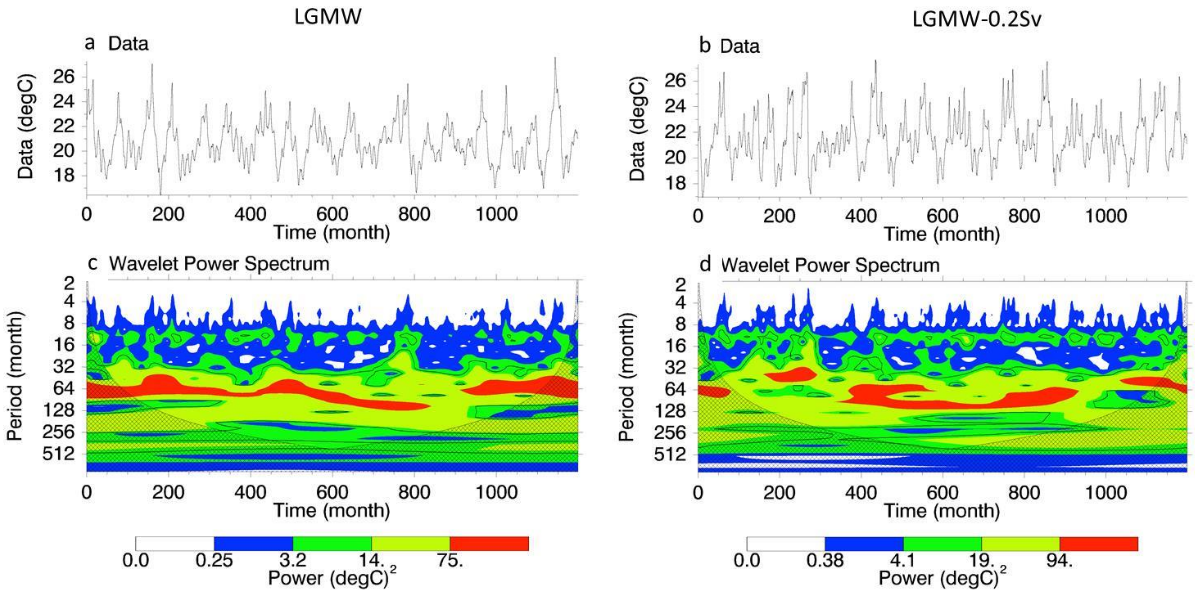

Fig.S7. The simulated seasonality of sea surface temperature (SST, °C) anomalies between the hosing experiment and the Last Glacial Maximum (LGM) control run in COSMOS (*S11*), i.e., December-January-February (DJF, upper left), March-April-May (MAM, upper right), June-July-August (JJA, lower left) and September-October-November (SON, lower right). The map was plotted by the Panoply (version 4.0, http://www.giss.nasa.gov/tools/panoply/).

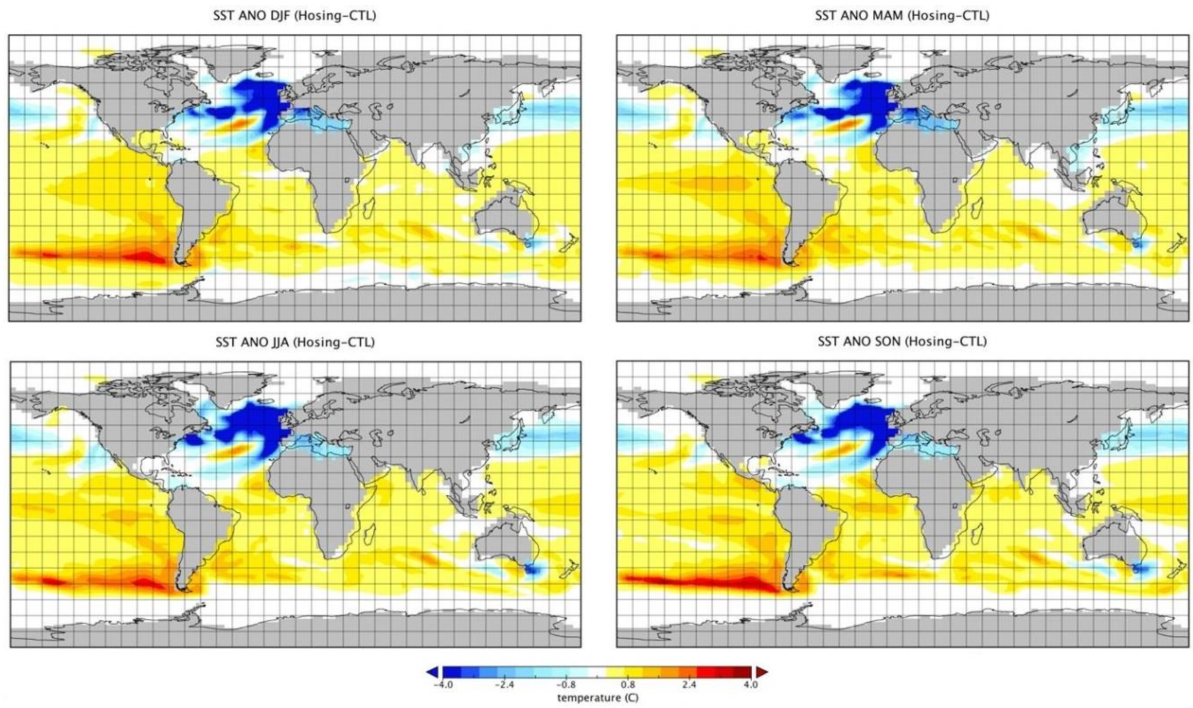

Fig.S8. Results of the atmospheric model sensitivity experiments with equatorial SST anomalies over different regions (other parameters are identical to our original EEP SST experiment), i.e., 180°W-70°W and 15°S-15°N (left), 140°E-70°W and 25°S-25°N (right). Climatology variables include rainfall (shaded, mm/day), 850hPa wind field (vectors, m/s) and sea level pressure (contours, Pa). This map was plotted by using Grid Analysis and Display System (GrADS, Version 2.0.2, http://cola.gmu.edu/grads/grads.php).

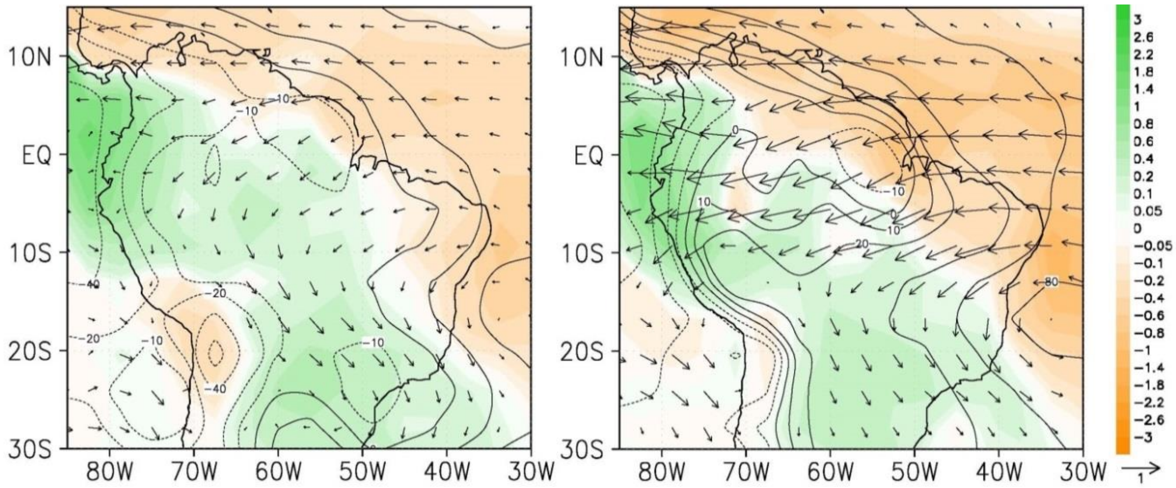

Fig.S9. Orography used in the atmospheric general circulation model (e.g., ECHAM5) to determine the peak of the Andes altitudes, which directly influences the atmospheric circulation pattern via atmospheric gravity wave. Unlike in regional climate models (e.g., Pennsylvania State University/National Center for Atmospheric Research (PSU/NCAR) MM5 (v3.6 model), see ref. *S14*), high resolution topography of the Andes cannot be resolved in this coarse-resolution version of ECHAM5. However, the more accurate altitudes of the Andes may promote the recycling process of the moisture from tropical western Atlantic, but will not lead to overestimation of the contribution of the Pacific Ocean and thus do not change our conclusion. The map was plotted by the Panoply (version 4.0, http://www.giss.nasa.gov/tools/panoply/).

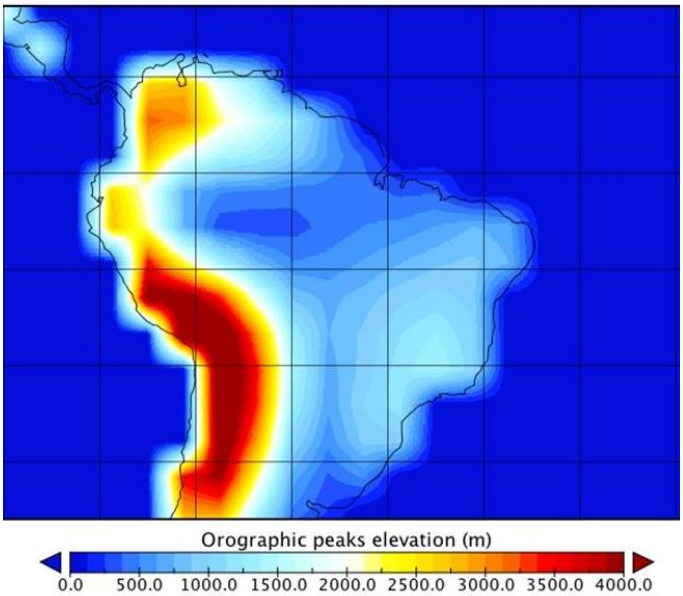

References

S1. Sanchez Goñi, M.F., Harrison, S. P. 2010. Millennial-scale climate variability and vegetation changes during the Last Glacial: Concepts and terminology. Quat. Sci. Rev. 29, 2823-2827.

S2. MARGO Project Members. 2009. Constraints on the magnitude and patterns of ocean cooling at the Last Glacial Maximum. Nature Geosciences 2, 127-132.

S3. Grosjean, M. et al. 2001. A 22,000 14C year BP sediment and pollen record of climate change from Laguna Miscanti (23°S), northern Chile. Global and Planetary Change 28(1-4), 35-51.

S4. Prado, L. F., Wainer, I., Chiessi, C. M., Ledru, M.P., Turcq, B. 2013. A mid-Holocene climate reconstruction for eastern South America. Clim. Past 9, 2117-2133

S5. D'Apolito, C., Absy, M. L., Latrubesse, E. M. 2013. The Hill of Six Lakes revisited new data and re-evaluation of a key Pleistocene Amazon site. Quat. Sci. Rev. 76, 140-155.

S6. Bush, M. B., De-Oliveira, P. E., Colinvaux, P. A., Miller, M. C., Moreno, J. E. 2004. Amazonian paleoecological histories: one hill, three watersheds. Palaeogeogr. Palaeoclimatol. Palaeoecol. 214, 359-393.

S7. Hermanowski, B., Marcondes, L. C., Hermann, B. 2012. Environmental changes in southeastern Amazonia during the last 25,000 yr revealed from a paleoecological record. Quaternary Res. 77, 138-148.

S8. Hermanowski, B., Marcondes, L. C., Hermann, B. 2015. Possible linkages of palaeofires in southeast Amazonia to a changing climate since the Last Glacial Maximum. Veget Hist Archaeobot 24, 279-292.

S9. Carneiro-Filho, A., Schwartz, D., Tatumi, S. H., Rosique, T. 2002. Amazonian Paleodunes Provide Evidence for Drier Climate Phases during the Late Pleistocene–Holocene. Quaternary Res. 58, 205-209 (2002).

S10. Rossetti D. F., Zani, H., Cohen, M. C. L., Cremon, É. H. 2012. A Late Pleistocene–Holocene wetland megafan in the Brazilian Amazonia. Sedimentary Geology 282, 276-293.

S11. Zhang, X., Lohmann, G. , Knorr, G. and Xu, X. 2013. Different ocean states and transient characteristics in the Last Glacial Maximum simulations and implications for deglaciation. Clim. Past 9, 2319-2333.

S12. Merkel, U., Prange, M., Schulz, M. 2010. ENSO variability and teleconnections during glacial climates. Quat. Sci. Rev. 29, 86-100.

S13. Liu, Z. et al. 2014. Evolution and forcing mechanisms of El Niño over the past 21,000 years. Nature 515, 550-553.

S14. Vizy, E. K., Cook, K. H. 2007. Relationship between Amazon and high Andes rainfall. J. Geophys. Res. 112, doi:10.1029/2006JD007980.